Dynamics of Formation of Products D_2CN^+, DCN^+, and CD_3^+ in the Reaction of N^+ with CD_4: A Crossed-Beam and Theoretical Study†

Jan Žabka,‡ Jana Roithová,‡,§,|| Patrik Španěl,‡ and Zdenek Herman*,‡

V. Čermák Laboratory, J. Heyrovsky Institute of Physical Chemistry, Academy of Sciences of the Czech Republic, Dolejškova 3, 18223 Prague 8, Czech Republic, Department of Organic Chemistry, Faculty of Sciences, Charles University in Prague, Hlavova 8, 12843 Prague 2, Czech Republic and Institute of Organic Chemistry and Biochemistry, Academy of Sciences of the Czech Republic, Flemingovo nám. 2, 16610 Prague 6, Czech Republic

Received: July 22, 2009; Revised Manuscript Received: September 9, 2009

The formation of D_2CN^+ in the reaction of N^+ (^3P) with CD_4 was studied using the crossed beam technique at collision energies of 3.66 and 4.86 eV. The experiments were complemented by calculations of stationary points on the triplet hypersurface of the system. The scattering data showed that the reaction proceeds by the formation of two intermediate complexes having different lifetimes: a long-lived statistical intermediate and a short-lived complex (mean lifetime about one period of an average rotation) with more energy in translation than the statistical complex. Comparison with theoretical calculations suggests that the long-lived complex leads the $CDND^+$ isomer of the product ion, whereas the short-lived complex leads prevailingly to the CD_2N^+ isomer. The product DCN^+ results from further decomposition of the primary product D_2CN^+, whereas CD_3^+ is formed both by a hydride-ion transfer and a long-lived complex decomposition.

Introduction

Beam scattering studies have provided useful and in many cases unique information on the dynamics of elementary ion−molecule reactions. A detailed description of the mechanisms of different reaction channels, the formation of different isomers, and the energy deposition in the products may be obtained by combining results of beam scattering studies with theoretical calculations of structures of the species involved and of stationary points on the respective potential-energy hypersurface.

One of the areas in which studies of ion−molecule reactions have been regarded as being of considerable importance is astrophysics because of the role these processes play in the interstellar space and planetary upper atmospheres. Recent spacecraft explorations of Mars, Jupiter, and Saturn and some of their moons have provided new data on their gaseous envelopes and initiated lively activity in modeling the atmospheres and ionospheres. A large amount of new data was obtained for Saturn's largest satellite Titan as a result of the previous missions of the Voyager spacecrafts and especially of the successful Cassini−Huygens spacecraft mission. The Voyager optical spectroscopy investigations indicated that Titan's atmosphere consisted largely of nitrogen (94%) and of hydrocarbons, mostly methane (6%). This led to the development of numerous models.[1] The Cassini−Huygens mission provided more detailed information on the atmosphere.[2,3] In particular, the Cassini ion and neutral mass spectrometer analyzed the neutral and ionic composition of the upper atmosphere and suggested a large importance of hydrocarbon and nitrile chains of reactions. Some of the ionic species observed (e.g., $HCNH^+$, $C_2H_5^+$, CH_5^+) were predicted by these models, and detections of others led to the emphasis on the nitrogen chemistry in the upper atmosphere.[4]

Formulation of the models of Titan's upper atmosphere requires reliable data on processes that occur between its constituents. Laboratory experiments on elementary processes between relevant particles represent one of the sources of the data. In this connection, ion−molecule reactions leading to nitrogen-containing species are of interest. Information on cross sections or rate constants of the elementary ion−molecule processes and branching ratios of various reaction channels are of prime importance. Moreover, detailed data on the dynamics of elementary processes may reveal valuable information on mechanisms of the processes in question, lifetimes of intermediate species involved, and pathways leading to different isomers of the products.

One of the simplest systems that deserves attention is a reaction between the atomic ion of nitrogen and methane, $N^+ + CH_4$. The reaction of the ground state $N^+(^3P)$ was found to yield four major reaction products, namely

$$N^+(^3P) + CH_4 \rightarrow CH_4^+ + N \quad (1a)$$

$$\rightarrow CH_3^+ + NH \quad (1b)$$

$$\rightarrow H_2CN^+ + H_2 \quad (1c)$$

$$\rightarrow HCN^+ + H_2 + H \quad (1d)$$

The branching ratio between these products has been previously determined by different methods. The first study[5] by the ion-cyclotron resonance (ICR) and tandem Dempster-ICR mass spectrometers gave the rate constant of 1.35×10^{-9} cm^3/s and the branching ratio $CH_4^+/CH_3^+/H_2CN^+/HCN^+ = 0.04:0.53:0.32:$

† Part of the "W. Carl Lineberger Festschrift".

* Corresponding author. E-mail: zdenek.herman@jh-inst.cas.cz.

‡ J. Heyrovsky Institute of Physical Chemistry, Academy of Sciences of the Czech Republic.

§ Charles University in Prague.

|| Institute of Organic Chemistry and Biochemistry, Academy of Sciences of the Czech Republic.

10.1021/jp9069493
Published on Web 10/07/2009

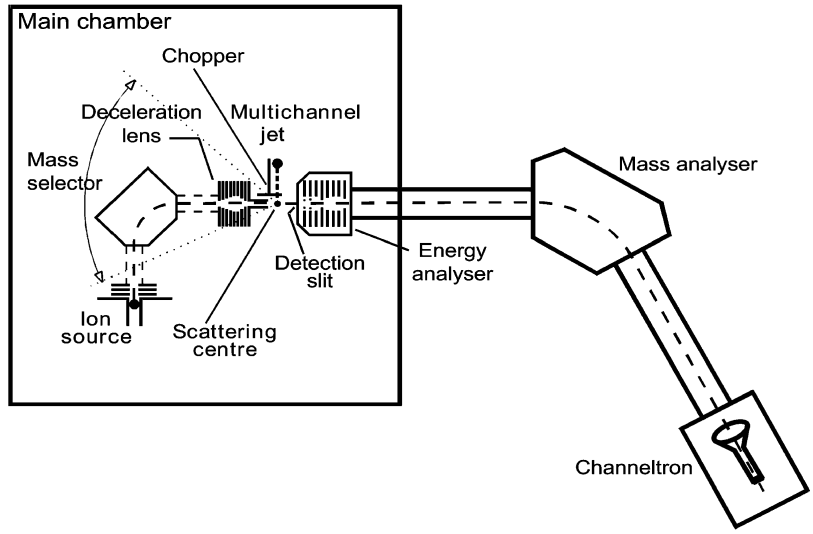

Figure 1. Schematic diagram of the crossed beam scattering apparatus EVA II.

0.10. A selected ion flow tube (SIFT) investigation at 300 K led to the rate constant of 9.4×10^{-9} cm^3/s and a very similar branching ratio 0.03:0.51:0.40:0.06.[6] Reactions of both ground (^3P) and excited metastable (^1S) states of N^+ were investigated in a SIFT study at 300 K, giving the rate constant of 1.1×10^{-9} cm^3/s and the product ratio 0.06:0.42:0.38:0.14 for the ground state and an inferred ratio of 0.10:0.20:0.40:0.30 for the metastable excited state.[7] A drift tube−mass spectrometric technique was used to study both the rate coefficient and the branching ratios.[8] The study gave very similar results as a subsequent tandem ICR investigation[9] of reactions relevant to Titan's atmosphere, namely, the branching ratio of reactions 1a−1d of $CH_4^+/CH_3^+/H_2CN^+/HCN^+ = 0.05:0.53:0.32:0.10$, which is in very good agreement with the earlier ICR data. Luminescence studies of the products of $N^+ + CH_4$ collisions showed emission of $NH^*(A^3\Pi)$,[10,11] indicating that at least a part of the product CH_3^+ originated in reaction 1b.

The reaction system $^{15}N^+ + CD_4$ was studied with a state-selected reactant ion prepared by dissociative photoionization of nitrogen using synchrotron radiation in coincidence with threshold photoelectrons.[12] The branching ratios of the deuterated analogues of 1a−1d were investigated in dependence on the collision energy of the projectile ions in the ground $N^+(^3P)$ state and the excited $N^+(^1D)$ states. Time-of-flight spectra of the product ions were obtained along the reactant ion direction, and axial velocity distributions were derived from them. Whereas the relative fractions of products of reactions 1c and 1d (formation of D_2CN^+ and DCN^+) did not depend much on the electronic state of the reactant ion, the branching ratio between reactions 1a and 1b was completely inverted in favor of charge transfer reaction 1a with $N^+(^1D)$. A plausible explanation of this phenomenon based on the spin−orbit selection rule in the N^+ recombination was suggested.

The present study concentrates mainly on detailed investigation of formation of D_2CN^+ in the reaction

$$N^+(^3P) + CD_4 \rightarrow D_2CN^+ + D_2 \qquad (2)$$

in crossed-beam scattering experiments. At the collision energy of 3.66 eV, angular distribution and translational energy distributions of the product ion were measured at a series of scattering angles, and from those a scattering diagram of D_2CN^+ was obtained. Center-of-mass (CM) angular distributions and relative translational energy distributions of the product ions from reaction 2 were then obtained by analysis of this scattering diagram. The experiments were complemented by theoretical calculations of stationary points on the triplet hypersurface of the system. Velocity profiles of DCN^+ and CD_3^+ at one scattering angle provided information on the mechanisms of the formation of these products. It should be noted that the present data on the dynamics of formation of the products were obtained at hyperthermal energies, whereas modeling of planetary atmospheres requires data in the thermal energy range.

Experimental Section

The experiments were carried out on the crossed beam apparatus EVA II (Figure 1). The performance and application of the machine to this type of scattering experiments has been previously described in detail many times. (See, e.g., refs 13 and 14.) Ground-state ions $N^+(^3P)$ were prepared by electron ionization of a mixture of He and N_2 ($He/N_2 \approx 10$) at relatively high ion source pressures ($\sim 10^{-2}$ Torr). Under these conditions, the N^+ ions are formed prevailingly by a fast dissociative charge transfer reaction

$$He^+(^2S) + N_2(X^1\Sigma_g^+) \rightarrow He(^1S) + N^+(^3P) + N(^4S) \qquad (3)$$

Reaction 3 is exoergic by −0.28 eV, whereas the reaction leading to the formation of the first excited state $N^+(^1D)$ is endoergic by 1.62 eV, and this ensures that the N^+ ions are formed in the ground state.[15] The ions were extracted from the ion source, mass analyzed, and decelerated by a multielement lens to the required laboratory energy. The N^+ beam was crossed at right angles with a beam of CD_4 molecules emerging from a multichannel jet. The ion beam had an angular and energy spread of 1.2° and 0.5 eV (full width at half-maximum (fwhm)), respectively; the collimated neutral beam had an angular spread of 6° (fwhm) and thermal energy distribution at 300 K. Reactant and product ions passed through a detection slit (2.5 cm from the scattering center) into a stopping potential-energy analyzer. They were then accelerated and focused into the detection mass spectrometer, mass analyzed, and detected with the use of a Galileo electron multiplier. Angular distributions were obtained by rotating the two beams about the scattering center. Modula-

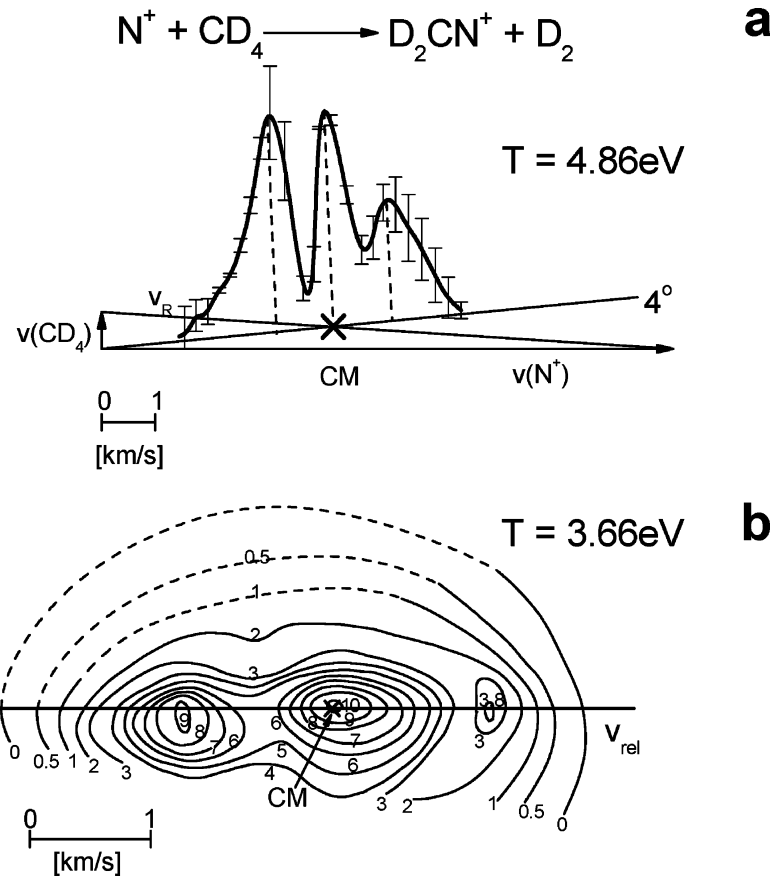

Figure 2. (a) Newton diagram with a velocity profile of D_2CN^+ from reaction 2 at the scattering angle of 4° and collision energy $T = 4.87$ eV. CM indicates the position of the center-of-mass of the system. (b) Contour scattering diagram of D_2CN^+ at $T = 3.66$ eV. The horizontal line indicates the direction of the relative velocity, v_{rel}.

tion of the neutral beam and phase-sensitive detection of the ion products was used to remove background scattering effects.

Laboratory angular distributions were repeatedly recorded, and the results were averaged. Energy profiles of the product ions were recorded three to six times at each of a series of laboratory scattering angles, the results were averaged, and the laboratory energy distributions were converted to velocity distributions. The laboratory angular and velocity distributions were used to construct the scattering diagram of the investigated product D_2CN^+. The contours in the scattering diagram refer to the Cartesian probability distribution[13,16] normalized to the maximum in the scattering diagram. The Cartesian probability distributions are proportional to the number of reactive events in an element of velocity space $dv_x\, dv_y\, dv_z = du_x\, du_y\, du_z$, the size of which is the same over the entire velocity space. (v and u are laboratory and CM velocities of the ion in question, respectively.) CM angular distributions (relative differential cross sections), $P(\vartheta_{CM})$ versus ϑ_{CM}, and relative translational energy distributions, $P(T')$ versus T', of the products were obtained by integrations of the scattering diagram, as previously described.[13,16]

Calculations

The theoretical calculations were performed using the hybrid density functional theory method B3LYP[17−19] in conjunction with the 6-311+G(2d,p) triple-ζ basis set, as implemented in the Gaussian 03 suite.[20] For all optimized structures, frequency analysis at the same level of theory was performed to assign them as genuine minima or transition structures on the potential-energy surface as well as to calculate zero-point vibrational energies (ZPVEs). All transition structures were further characterized by an intrinsic reaction coordinate calculation.[21,22] Relative energies (E_{rel}) are given at 0 K and are anchored to the energy of reactants $E^{0K}(N^+ + CH_4) = -94.551767$ hartree.

Results and Discussion

Experiment: Formation of D_2CN^+. Figure 2a shows the Newton diagram of the system $N^+ + CD_4$ at the collision energy of 4.86 eV with the measured velocity profile of the product D_2CN^+ along the laboratory scattering angle of 4°, approximately across the CM of the system. The velocity distribution of D_2CN^+ exhibits features similar to the velocity distribution of the corresponding product of the $^{15}N^+ + CD_4$ reaction reported in ref 12. Note that the velocity profile in ref 12 was obtained at the collision energy of 1.0 eV from the time-of-flight spectra of D_2CN^+ from reaction 2 measured along the velocity of the reactant beam (corresponding to the scattering angle $\vartheta_{CM} = 0°$) using a quadrupole−double octupole−quadrupole device with a collision cell and exhibits three not fully resolved peaks in the vicinity of the CM of the system. In our velocity distribution (Figure 2a), the central peak is located within the experimental error at the CM, and the two outer peaks, somewhat better resolved than in ref 12, are located equidistantly (±1.1 km/s) forward and backward with respect to the center of mass, with the backward peak about twice as large as the forward outer peak.

Figure 2b shows the full scattering diagram of D_2CN^+ from reaction 2 at the collision energy of 3.66 eV obtained as described in the previous section. The central peak is located directly at the CM, and the forward and backward outer peaks

are at a distance of 1.25 km/s from it. In agreement with the results above, the outer backward peak has more than two-fold intensity compared with the forward peak.

The shape and structures of the scattering diagram imply formation of the product D_2CN^+ in reaction 2 via two mechanisms. One of them is responsible for the central structure of the scattering diagram at the CM, and this feature is consistent with a formation of a long-lived intermediate complex (central structure peaking at the CM) of a mean lifetime exceeding many average rotations of such species. The other mechanism is connected to the scattered product ions forming the two peaks of different intensity symmetrically located forward and backward with respect to the CM; the more intense peak is in the backward direction. This behavior is consistent with the formation of a shorter-lived complex. The incomplete development of the forward−backward symmetry of the short-lived complex results from the mean lifetime of the intermediate being only about one or a few average rotations of the intermediate. Analogous problems of two complexes of different lifetimes in ion−molecule reactions have been previously treated by us.[23,24] In those cases, however, the preferential peaking of products formed by decomposition of the short-lived complex was in the direction of the movement of the approaching ion reactant, that is, forward with respect to the CM. Such behavior can be rationalized by following the development of the forward−backward symmetry, assuming at least approximately statistical (exponential distribution of lifetimes) decay of a complex rotating with a certain average period.[23] If the mean lifetime is comparable to one average rotational period of the decomposing complex, then the larger part of dissociation occurs during the first half-period of an average rotation than during the second half-period. This results in more product ions recoiling forward than backward with respect to the direction of the movement of the ion reactant. This forward−backward asymmetry gradually decreases as the mean lifetime increases from about one to several average rotational periods and eventually disappears if the mean lifetime of the decomposing complex exceeds about six to seven average rotations.[23]

However, in the case of D_2CN^+ formation via the short-lived complex, one has just the opposite case (Figure 2a,b), namely, the more intense outer peak is in the backward direction. This feature may be explained assuming that a nonadiabatic transition, an electron exchange process

$$N^+(^3P) + CD_4 \rightarrow N(^4S) + CD_4^+ \qquad (4)$$

occurs in the entrance valley between the approaching reactants as a first step in the interparticle interaction. The charge transfer reaction 4 is exoergic by 2.03 eV,[25] the charge transfer products are among the reaction products in the system (reaction 1a), and thus this assumption is quite plausible. The formation of the short-lived complex then occurs between CH_4^+ and neutral N, and the product peaks preferentially in the direction of the approaching ion reactant. An electron transfer, an adiabatic transition in the entrance valley of the reactants, is nothing exceptional. A combination of electron transfer and hydrogen atom transfer process was previously postulated in theoretical calculations of CH_5^+ formation in $CH_4^+ + CH_4$ collisions,[26,27] and nonadiabatic transitions in the reactant valley were shown theoretically to be important in the formation of ArH^+ in the $Ar^+ + H_2$ reaction.[28]

CM angular distribution, $P(\vartheta_{CM}) - \vartheta_{CM}$, of the product D_2CN^+ from reaction 2 at $T = 3.66$ eV was obtained by the

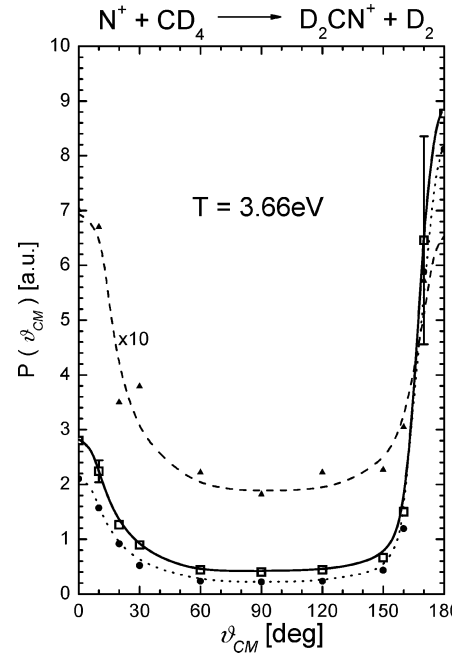

Figure 3. Center-of-mass (CM) angular distribution, $P(\vartheta_{CM}) - \vartheta_{CM}$, of D_2CN^+ at $T = 3.66$ eV. Open squares and solid line: integration over the entire scattering diagram in Figure 2b; triangles and dashed line: integration over the deconvoluted central part of the scattering diagram (long-lived complex); solid points and dotted line: integration over the deconvoluted outer parts of the scattering diagram (short-lived complex).

usual integration of the scattering diagram in Figure 2b, and it is given in Figure 3. It shows strong peaking with maxima at 180 and 0°, the value at 0° (forward direction) being only ∼32% of that at 180° (backward direction), and a small value of ∼5% of the maximum $P(\vartheta_{CM})$ value at scattering angles of ∼90°. The velocity profiles at different scattering angles ϑ_{CM} in the scattering diagram (Figure 2b) were approximately deconvoluted to yield separately the components connected to the central peak and to the two outer peaks, and the results were integrated to obtain approximate deconvolution of the CM angular distributions pertaining to the central and outer peaks. The deconvolution is shown in Figure 3 by dashed (central peak) and dotted lines (outer forward and backward peaks).

The angular distribution connected with the central peak shows symmetric forward and backward peaking at 0 and 180° with a decrease to ∼27% of the peak value at scattering angles of ∼90° (perpendicular to the relative velocity). This shape implies an intermediate that is prolate in its critical configuration and has a mean lifetime exceeding at least six average rotations[23] of such a species before it decomposes to the products of reaction 2.

The angular distribution relevant to the scattering giving rise to the two uneven outer peaks is shown by the dotted line. It is very strongly pointed in the backward and forward direction, with the forward peak ∼25% of the main backward peak at 180° and a very low intensity of ∼3% of the backward peak at $\vartheta_{CM} = 90°$. This indicates a prolate short-lived intermediate. By comparing the ratio Z of the integrals $P(\vartheta)$ of particles scattered into the forward and backward direction[23]

$$Z = \left(\int_{0^\circ}^{90^\circ} P(\vartheta) \sin\vartheta \, d\vartheta\right) / \left(\int_{90^\circ}^{180^\circ} P(\vartheta) \sin\vartheta \, d\vartheta\right) \qquad (5)$$

one obtains for the short-lived complex $Z = 0.68$, and this corresponds to the average lifetime of the intermediate about one average rotational period.[23]

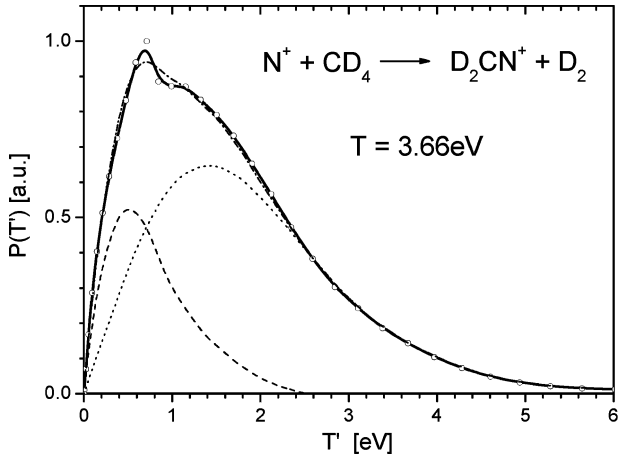

Figure 4. Relative translational energy distribution, $P(T') - T'$, of the products $D_2CN^+ + D_2$ at $T = 3.66$ eV, as derived from the scattering diagram in Figure 2b (open points and solid line). Dashed line: calculations for a long-lived statistical complex;[29] dotted line: remaining part of the distribution after subtracting the calculated contribution of the statistical complex; dash-and-dotted line: sum of dashed and dotted lines.

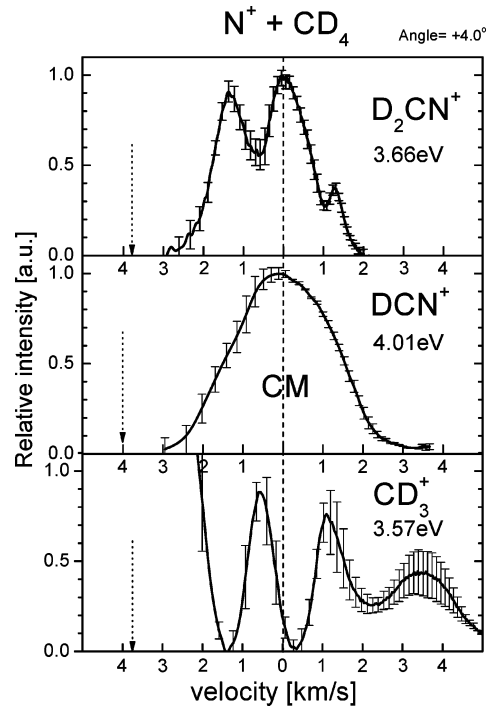

Figure 5. Velocity profiles of D_2CN^+, DCN^+, and CD_3^+ at the scattering angle of +4°; collision energies indicated in the figures. CM: position of the center-of-mass; dotted line with an arrow: position of the origin of the Newton diagram. (See Figure 2a.)

The relative translational energy distribution of the products, $P(T') - T'$, as derived from the scattering diagram in Figure 2b, is given in Figure 4 (points and solid line). The distribution shows a low energy peak and a higher energy shoulder, evidently connected to the central peak and the two outer maxima in the scattering diagram in Figure 2b. A deconvolution of the summary $P(T')$ curve was carried out by using the Klots model of a statistical complex decomposition,[29] and this led to the dashed curve in Figure 4 that peaks at 0.5 eV and decreases gradually to zero at ~2.5 eV. The remaining part of the distribution is shown by the dotted line, peaking at ~1.4 eV. The deconvoluted curve at lower $P(T')$ is related to the translational energy release in the decomposition of a statistical complex that corresponds to the central peak in the scattering diagram (Figure 2b) and the deconvoluted CM angular distribution of the long-lived complex. The deconvoluted curve peaking at 1.4 eV corresponds to the outer structures in the scattering diagrams and to the CM angular distribution of the intermediate of a short mean lifetime (dashed line in Figure 3). Integration of the areas under the deconvoluted curves of $P(T')$ in Figure 4 leads to the relative contributions of the long-lived complex decomposition to the short-lived complex decomposition to the overall formation of the product D_2CN^+ of 0.25:0.75. This is in reasonable agreement with the value of this ratio obtained from the integration of the deconvoluted angular distributions of 0.33:0.66.

Therefore, the experimental evidence indicates that the formation of the product D_2CN^+ in reaction 2 involves two different pathways, a decomposition of a long-lived statistical complex that gives rise to the central structure in the scattering diagram, the forward−backward symmetric contribution to the CM angular distribution, and to the low-energy contribution of $P(T')$, which is consistent with the distribution expected from a long-lived statistical complex decomposition. The decomposition of a short-lived complex (estimated mean lifetime of about one average rotational period) gives rise to the two outer structures in the scattering diagram, the asymmetric contribution to the CM angular distribution, peaking in the backward direction, and to the higher-energy contribution to the $P(T')$ curve, peaking at about 1.4 eV. Calculation of the stationary points on the hypersurface of the system $N^+ + CH_4$ shows (see later) that the decomposition of two different complexes can be identified with different pathways on the hypersurface, leading to two different isomers of the product ion D_2CN^+.

Experiment: Formation of DCN^+ and CD_3^+. For the remaining channels of reaction (1a−1d), we have much less scattering information, and the results make only qualitative conclusions possible. Figure 5 shows the velocity profiles of D_2CN^+, DCN^+, and CD_3^+ from the reaction of $N^+(^3P)$ with CD_4, measured at the laboratory scattering angle of +4° (approximately along the CM velocity of the reactants) and at about the same collision energy. The intensity scale in Figure 5 is relative and does not reflect the actual intensity of the product ions. The velocity profile of D_2CN^+ in Figure 5 is one of the velocity profiles used to construct the scattering diagram of D_2CN^+ in Figure 2b.

The analogue of reaction 1d, the reaction of DCN^+ formation

$$N^+(^3P) + CD_4 \rightarrow DCN^+ + D + D_2 \qquad (6)$$

is exoergic by 1.40 eV, and DCN^+ is one of the product channels even at thermal collision energies.[6] The velocity profile of DCN^+ in Figure 5 shows that its velocity peaks at the CM and decreases toward zero at about ±3 km/s. This behavior suggests that DCN^+ is a secondary product formed by the decomposition of the primary product D_2CN^+ by the emission of one D atom. The translational energy release in the dissociation process smears out structures in the DCN^+ profile, but it is evident that the product D_2CN^+ appearing close to the CM (connected to the central structure in the velocity profile of this ion) dissociates more efficiently than the product D_2CN^+ appearing in the wings of the D_2CN^+ velocity profile (connected to the outer peaks). This finding is in qualitative agreement with the relative translational energy distribution of the products (Figure 4): the deconvoluted curve of $P(T')$ connected to the low-energy part

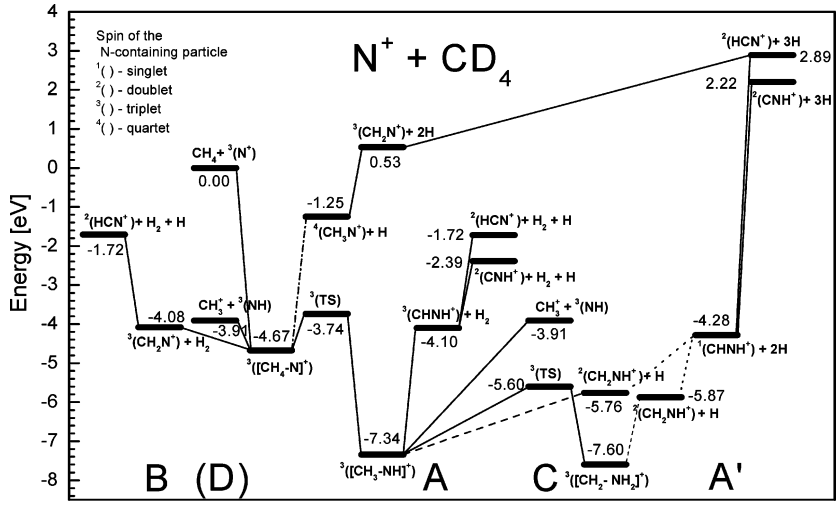

Figure 6. Theoretical calculations: Stationary points on the potential-energy hypersurface of the system $N^+(^3P) + CD_4$. Upper indices with species in parentheses indicate the spin of the N-containing particle; letters in the lower part of the diagram refer to various pathways, as discussed in the text.

of the distribution and decomposition of the long-lived complex channels only 0.5 eV (peak value) into translational energy and leaves more internal energy in the product pair $D_2CN^+ + D_2$ than the decomposition of the short-lived complex, where the peak value of the fraction of energy in translation is 1.5 eV.

The lower part of Figure 5 shows the velocity profile of CD_3^+ formed in the analogue of reaction 1b

$$N^+(^3P) + CD_4 \rightarrow CD_3^+ + ND \qquad (7)$$

The velocity profile shows a steep rise to a very strong peak in the backward direction, presumably located at ~3 km/s, at a very low energy on the laboratory energy scale that could not be reliably measured in our experiments, a pair of almost symmetric peaks forward and backward with respect to the CM, with the experimental error ~1 km/s from the CM, and a weak peak forward with respect to the CM (at ~3.4 km/s). The strong backward peak in Figure 5 evidently corresponds to the peak at the laboratory velocity of 0.1 km/s described by the authors of ref 12 (Figure 5f of this reference) as the product CD_3^+ formed by hydride-ion transfer, dissociative charge transfer, or both. This hydride-ion transfer requires the formation of a short-lived collision species,[30,31] and the peak at 3.4 km/s in Figure 5 corresponds presumably to the backward peak related to it. Of interest are the two symmetric peaks near the CM that imply that a small amount of the CD_3^+ product is formed by an intermediate complex decomposition. This reaction pathway was not previously described. The position of the two peaks with respect to the CM indicates a translational energy release of about 0.15 to 0.2 eV, a small value consistent with a long-lived complex formation and decomposition that channels only a small fraction of the total energy available into translational energy of the products. The relative importance of the long-lived complex formation, with respect to the hydride-ion transfer, may increase with decreasing collision energy.

Calculations. Theoretical calculations were carried out for the system $N^+ + CH_4$; therefore, we refer to H instead of D in connection with theory, thus neglecting any possible isotope effects. The theoretical calculations reveal that the formation of the collision complex $^3(CH_4N^+)$ (superscript 3 denotes that the complex is considered in the triplet state; by analogy, 1 corresponds to the singlet state, and 2 corresponds to the doublet state) from the reactants $^3(N^+)$ and CH_4 releases 4.67 eV of energy (Figure 6). This internal energy is available for surmounting numerous reaction barriers and forming different products. The most straightforward reaction pathway corresponds to the decomposition of $^3(CH_4{-}N^+)$ either to $^3(CH_2{-}N^+) + H_2$ ($\Delta E_{rel,0K} = -4.08$ eV, pathway B) or $CH_3^+ + {}^3(NH)$ ($\Delta E_{rel,0K} = -3.91$ eV, pathway D). An alternative pathway to B is the successive loss of two hydrogen atoms, which is endothermic ($\Delta E_{rel,0K} = 0.53$ eV) but still conceivable in experiments carried out at sufficiently large collision energies.

In addition to these decompositions, the collision complex $^3(CH_4{-}N^+)$ can undergo a rearrangement to a pool of more stable intermediates $^3(CH_3{-}NH)^+$ ($\Delta E_{rel,0K} = -7.34$ eV) and $^3(CH_2{-}NH_2^+)$ ($\Delta E_{rel,0K} = -7.60$ eV). Several decomposition pathways are then opened. First, both of these intermediates can lose a H_2 molecule and form products $^3(CHNH^+) + H_2$ ($\Delta E_{rel,0K} = -4.10$ eV, pathway A). However, an even more probable process seems to be the subsequent loss of two H atoms shown to be a prevailing mechanism in the dissociation of internally excited small amines.[32] Therefore, most likely, both intermediates (i.e., $^3(CH_3{-}NH^+)$ and $^3(CH_2{-}NH_2^+)$) are likely to lose sequentially two hydrogen atoms and form $^1(CHNH^+)$ ($\Delta E_{rel,0K} = -4.28$ eV, pathway A′). Another fragmentation of the intermediate $^3(CH_3NH^+)$ is the C−N bond cleavage to form $CH_3^+ + {}^3(NH)$ ($\Delta E_{rel,0K} = -3.91$ eV, pathway C).

Finally, we can also address processes leading to the product HCN^+. It appears that $^2(HCN^+)$ is formed in the pathway B by the decomposition of the product $^3(CH_2{-}N^+)$. In pathway A, both $^2(HCN^+)$ and $^2(CNH^+)$ can be formed by decomposition of the product $^2(CHNH^+)$. All of these processes are exothermic with respect to the reactants. There remains a possibility of forming HCN^+ or CNH^+ by a sequential shake-off of three H-atoms in endothermic processes (by 2.89 or 2.22 eV, respectively) at higher collision energies.

Comparison of Experimental and Theoretical Results. The above-mentioned experimental and theoretical results make it possible to suggest pathways on the potential-energy surface of the system that correspond to the experimental findings on the scattering of the D_2CN^+ product ion. (In the following, we use H instead of D when referring to the results of calculations and Figure 6.) The formation of D_2CN^+ via a long-lived complex (central part of the scattering diagram) may be identified with pathway A on the potential-energy surface

(Figure 6) going from the reactants through a shallow minimum $^3(CH_4-N^+)$ and a transition state at −3.74 eV to a deep minimum of the triplet complex $^3(CH_3-NH^+)$ (−7.34 eV) and to the products $^3(CHNH^+) + H_2$ with overall exothermicity of −4.10 eV (pathway A). The deep minimum is consistent with the formation of the long-lived complex. The other possibility, which is consistent with the formation of a long-lived complex, is pathway A′ leading to singlet $^1(CHNH^+)$ via subsequent shake-off of two H-atoms (pathway A′ via intermediates $^3(CH_3-NH^+)$ or $^3(CH_2-NH_2^+)$).

The formation of D_2CN^+ via the short-lived complex can be connected to pathway B, leading to the triplet intermediate CH_4-N^+ at −4.67 eV and from it to the products CH_2N^+ (triplet) + H_2 at −4.08 eV. The shallow minimum on this pathway, 0.59 eV below the energy of the products, suggests a short-lived intermediate.

A simple rough estimation of the mean lifetimes of the two complexes, τ (in seconds), using the RRK model in the form $\tau = 1/k \approx 10^{-13}(E - E_0/E)^{1-s}$ (where E is the total energy of the complex, E_0 is the barrier for decomposition of the intermediate toward the reactants, and s is the number of internal degrees of freedom of the intermediate) and the available energetics from Figure 6 lead to the ratio of the two mean lifetimes $\tau_L/\tau_S = 10-20$, which is in general agreement with the experimental findings (lifetime of the long-lived complex, τ_L, of more or much more that six average rotations vs lifetime of the short-lived complex, τ_S, of about one average rotation).

This reasoning leads us to the conclusion that two different isomers D_2CN^+ can be formed in reaction 2 by the decomposition of different intermediates: the decomposition of a long-lived intermediate complex leads to the product $CHNH^+$ via the pathways A and A′ on the potential-energy surfaces, whereas the decomposition of a short-lived complex leads to CH_2N^+ isomer via pathway B. On average, the product CH_2N^+ will have more energy in translation, although both channels have about the same exothermicity (−4.08 vs −4.10 and −4.28 eV for pathway A′).

The product HCN^+ evidently results from secondary decomposition of the reaction products $^3[CH_2-N]^+$ and $^3[CHNH]^+$ by the dissociation of one of the hydrogen atoms; evidently, only $^2[HCN^+]$ can be formed from the former, whereas from the latter two isomers, $^2[HCN^+]$ and $^2[CNH^+]$, may be formed. Subsequent splitting-off of three H atoms is possible but presumably less likely because of the endothermicity of the process.

Finally, theoretical calculations justify the possibility of the formation of CH_3^+ via a long-lived complex, as observed in the experiments. Pathway C leading to the products $CH_3^+ + {}^3[NH]$ (at −3.91 eV) goes through a deep minimum of the intermediate $^3[CH_3NH]^+$ that makes the formation of a long-lived intermediate possible.

Conclusions

(1) Scattering experiments showed that the formation of D_2CN^+ in the reaction of $N^+(^3P)$ with CD_4 involves two types of intermediate complexes having different mean lifetimes. The comparison with theoretical calculations of stationary points on the respective hypersurface showed that the decomposition of the long-lived statistical complex proceeds via the formation of intermediates (CD_4N^+) and more stable isomers (CD_3ND^+) and ($CD_2ND_2^+$) and by the release of D_2 or by the subsequent release of two D atoms leading preferentially to the isomer $CDND^+$ (∼30% of the total amount of the product D_2CN^+). The decomposition of the short-lived complex (CD_4N^+) leads directly to the isomer CD_2N^+ by the release of D_2. (2) The product DCN^+ results from secondary decomposition of the products $CDND^+$ or CD_2N^+. (3) A small amount of the product CD_3^+ is formed, besides the previously described prevailing formation by hydride-ion transfer, by decomposition of a long-lived intermediate $[CD_2ND]^+$.

Acknowledgment. It is a great pleasure to dedicate this article to W. Carl Lineberger, an old friend and respected colleague, in appreciation of his numerous contributions to the development of molecular and chemical physics. Partial support of the experimental research by the Grant Agency of the Academy of Sciences of the Czech Republic (grant no. IA400400702) and of the theoretical calculations by the Ministry of Education of the Czech Republic (MSM0021620857) is gratefully acknowledged.

References and Notes

(1) Cravens, T. E.; Vann, J.; Clark, J.; Yu, J.; Keller, C. N.; Brull, C. *Adv. Space Res.* **2004**, *33*, 212, and references cited therein.
(2) Waite, J. H., Jr.; Cravens, T. E.; Ip, W.-H.; Kasprzak, W. T.; Luhmann, J. G.; McNutt, R. L.; Niemann, H. B.; Yelle, R. V.; Mueller-Wodarg, I.; Ledvina, S. A.; Scherer, S. *Science* **2005**, *307*, 1260.
(3) Cravens, T. E.; Robertson, I. P.; Waite, J. H.; Yelle, R. V.; Kasprzak, W. T.; Keller, C. N.; Ledvina, S. A.; Niemann, H. B.; Luhmann, J. G.; McNutt, R. L.; Ip, W.-H.; De La Haye, V.; Mueller-Wodarg, I.; Wahlund, J.-E.; Anicich, V. G.; Vuitton, V. *Geophys. Res. Lett.* **2006**, *33*, L07105.
(4) Vuitton, V.; Yelle, R. V.; Anicich, V. G. *Astrophys. J.* **2006**, *647*, L175. and references therein.
(5) Anicich, V. G.; Huntress, W. T.; Futrell, J. H. *Chem. Phys. Lett.* **1977**, *47*, 488.
(6) Smith, D.; Adams, N. G.; Miller, T. M. *J. Chem. Phys.* **1978**, *69*, 308.
(7) Tichý, M.; Rakshit, A. B.; Lister, D. G.; Twiddy, N. D.; Adams, N. G.; Smith, D. *Int. J. Mass Spectrom Ion Phys.* **1979**, *29*, 231.
(8) Dheandhanoo, N. G.; Johnsen, R.; Biondi, M. A. *Planet. Space Sci.* **1984**, *32*, 1301.
(9) McEwan, M. J.; Scott, G. B. I.; Anicich, V. G. *Int. J. Mass Spectrom Ion Processes* **1998**, *172*, 209–219.
(10) Kusunoki, I.; Ottinger, C. *J. Chem. Phys.* **1979**, *70*, 699.
(11) Kusunoki, I.; Ottinger, C. *J. Chem. Phys.* **1979**, *70*, 710.
(12) Alcaraz, C.; Nicolas, C.; Thissen, R.; Žabka, J.; Dutuit, O. *J. Phys. Chem. A* **2004**, *108*, 9998.
(13) Herman, Z. *Int. J. Mass Spectrom.* **2001**, *212*, 413.
(14) Žabka, J.; Dolejšek, Z.; Hrušák, J.; Herman, Z. *Int. J. Mass Spectrom. Ion Processes* **1999**, *185/186/187*, 195.
(15) Tully, J. C.; Herman, Z.; Wofgang, R. *J. Chem. Phys.* **1971**, *54*, 1730.
(16) Friedrich, B.; Herman, Z. *Collect. Czech. Chem. Commun.* **1984**, *49*, 570.
(17) Vosko, S. H.; Wilk, L.; Nusair, M. *Can. J. Phys.* **1980**, *58*, 1200.
(18) Lee, C.; Yang, W.; Parr, R. G. *Phys. Rev. B* **1988**, *37*, 785.
(19) Miehlich, B.; Savin, A.; Stoll, H.; Preuss, H. *Chem. Phys. Lett.* **1989**, *157*, 200.
(20) Frisch, M. J.; Trucks, G. W.; Schlegel, H. B.; Scuseria, G. E.; Robb, M. A.; Cheeseman, J. R.; Montgomery, J. A., Jr.; Vreven, T.; Kudin, K. N.; Burant, J. C.; Millam, J. M.; Iyengar, S. S.; Tomasi, J.; Barone, V.; Mennucci, B.; Cossi, M.; Scalmani, G.; Rega, N.; Petersson, G. A.; Nakatsuji, H.; Hada, M.; Ehara, M.; Toyota, K.; Fukuda, R.; Hasegawa, J.; Ishida, M.; Nakajima, T.; Honda, Y.; Kitao, O.; Nakai, H.; Klene, M.; Li, X.; Knox, J. E.; Hratchian, H. P.; Cross, J. B.; Adamo, C.; Jaramillo, J.; Gomperts, R.; Stratmann, R. E.; Yazyev, O.; Austin, A. J.; Cammi, R.; Pomelli, C.; Ochterski, J. W.; Ayala, P. Y.; Morokuma, K.; Voth, G. A.; Salvador, P.; Dannenberg, J. J.; Zakrzewski, V. G.; Dapprich, S.; Daniels, A. D.; Strain, M. C.; Farkas, O.; Malick, D. K.; Rabuck, A. D.; Raghavachari, K.; Foresman, J. B.; Ortiz, J. V.; Cui, Q.; Baboul, A. G.; Clifford, S.; Cioslowski, J.; Stefanov, B. B.; Liu, G. Liashenko, A.; Piskorz, P.; Komaromi, I.; Martin, R. L.; Fox, D. J.; Keith, T.; Al-Laham, M. A.; Peng, C. Y.; Nanayakkara, A.; Challacombe, M.; Gill, P. M. W.; Johnson, B.; Chen, W.; Wong, M. W.; Gonzalez, C.; Pople, J. A. *Gaussian 03*, revision C.02; Gaussian, Inc.: Wallingford, CT, 2004.
(21) Gonzalez, C.; Schlegel, H. B. *J. Chem. Phys.* **1989**, *90*, 2154.
(22) Gonzalez, C.; Schlegel, H. B. *J. Phys. Chem.* **1990**, *94*, 5523.
(23) Friedrich, B.; Herman, Z. *Chem. Phys.* **1982**, *69*, 433–442.
(24) Žabka, J.; Dutuit, O.; Dolejšek, Z.; Polách, J.; Herman, Z. *Phys. Chem. Chem. Phys.* **2000**, *2*, 781.
(25) Lias, S. G.; Bartmess, J. E.; Liebmann, J. F.; Holmes, J. L.; Levin, R. D.; Mallard, W. C. *J. Phys. Chem. Ref. Data* **1988**, *17*, Suppl. 1.

(26) Kamiya, K.; Morokuma, K. *Chem. Phys. Lett.* **1986**, *123*, 331.
(27) Herman, Z.; Henchman, M.; Friedrich, B. *J. Chem. Phys.* **1990**, *93*, 4916.
(28) Chapman, S.; Preston, R. K. *J. Chem. Phys.* **1974**, *60*, 650.
(29) Klots, C. E.; Polách, J. *J. Phys. Chem.* **1995**, *99*, 15396.
(30) Fárník, M.; Dolejšek, Z.; Herman, Z.; Bondybey, V. *Chem. Phys. Lett.* **1993**, *216*, 458.
(31) Žabka, J.; Fárník, M.; Dolejšek, Z.; Polách, J.; Herman, Z. *J. Phys. Chem.* **1995**, *99*, 15595.
(32) Roithová, J.; Schröder, D.; Schwarz, H. *Eur. J. Org. Chem.* **2005**, *15*, 3304.

JP9069493